SCIENTIFIC REPORTS

OPEN

Received: 22 May 2019
Accepted: 9 July 2019
Published online: 18 July 2019

# Comparison of chemical stability and corrosion resistance of group IV metal oxide films formed by thermal and plasma-enhanced atomic layer deposition

Min Li, Zhi-Xian Jin, Wei Zhang, Yu-Hang Bai, Yan-Qiang Cao, Wei-Ming Li, Di Wu & Ai-Dong Li

**The wide applications of ultrathin group IV metal oxide films ($TiO_2$, $ZrO_2$ and $HfO_2$) probably expose materials to potentially reactive etchants and solvents, appealing for extraordinary chemical stability and corrosion resistance property. In this paper, $TiO_2$ ultrathin films were deposited on Si at 200 °C while $ZrO_2$ and $HfO_2$ were grown at 250 °C to fit their growth temperature window, by thermal atomic layer deposition (TALD) and plasma-enhanced ALD (PEALD). A variety of chemical liquid media including 1 mol/L $H_2SO_4$, 1 mol/L HCl, 1 mol/L KOH, 1 mol/L KCl, and 18 MΩ deionized water were used to test and compare chemical stability of all these as-deposited group IV metal oxides thin films, as well as post-annealed samples at various temperatures. Among these metal oxides, TALD/PEALD $HfO_2$ ultrathin films exhibit the best chemical stability and anti-corrosion property without any change in thickness after long time immersion into acidic, alkaline and neutral solutions. As-deposited TALD $ZrO_2$ ultrathin films have slow etch rate of 1.06 nm/day in 1 mol/L HCl, however other PEALD $ZrO_2$ ultrathin films and annealed TALD ones show better anti-acid stability, indicating the role of introduction of plasma $O_2$ in PEALD and post-thermal treatment. As-deposited $TiO_2$ ultrathin films by TALD and PEALD are found to be etched slowly in acidic solutions, but the PEALD can decrease the etching rate of $TiO_2$ by ~41%. After post-annealing, $TiO_2$ ultrathin films have satisfactory corrosion resistance, which is ascribed to the crystallization transition from amorphous to anatase phase and the formation of 5% Si-doped $TiO_2$ ultrathin layers on sample surfaces, i.e. Ti-silicate. $ZrO_2$, and $TiO_2$ ultrathin films show excellent corrosion endurance property in basic and neutral solutions. Simultaneously, 304 stainless steel coated with PEALD-$HfO_2$ is found to have a lower corrosion rate than that with TALD-$HfO_2$ by means of electrochemical measurement. The pre-treatment of plasma $H_2$ to 304 stainless steel can effectively reduce interfacial impurities and porosity of overlayers with significantly enhanced corrosion endurance. Above all, the chemical stability and anti-corrosion properties of IV group metal oxide coatings can be improved by using PEALD technique, post-annealing process and plasma $H_2$ pre-treatment to substrates.**

Group IV metal oxide films deposited via atomic layer deposition (ALD) including titania ($TiO_2$), zirconia ($ZrO_2$) and hafnia ($HfO_2$) have been widely investigated due to their excellent properties in electrical, optical, photocatalytical, biological and mechanical fields[1–6]. During certain utilization process, these films have to work in harsh environments such as chemical liquid media of acid and alkaline with a wide range of pH value to maintain their desired properties. ALD is a competitive technique for thin film deposition based on sequential self-limited reaction mechanism using precursor vapor, which has many unique advantages such as large area

National Laboratory of Solid State Microstructures, Department of Materials Science and Engineering, College of Engineering and Applied Sciences, Collaborative Innovation Center of Advanced Microstructures, Nanjing University, Nanjing, 210093, People's Republic of China. Correspondence and requests for materials should be addressed to A.-D.L. (email: adli@nju.edu.cn)

uniformity, excellent three-dimensional conformality, simple and precise control in film thickness, dense and pinhole-free films, and low processing temperature[7,8]. Compared with the conventional thermal ALD (TALD), plasma-enhanced ALD (PEALD) is an energy-assisted method for fabrication of thin films, where plasma species are utilized as reactive gas during one step of the cyclic deposition process[9]. It can produce some virtues over the TALD route, including more choice of materials and precursors, substrate temperature at room temperature, improved film density and quality with high purity and little defects, etc.[10]. Therefore, extensive and intensive studies on ALD-derived ultrathin films as protective coatings and anti-corrosion barriers are needed greatly. In consideration of better film quality, PEALD may be the more suitable candidate to obtain the ultrathin corrosion-resistant coatings with long-term stability in severe environments[11,12].

So far, some researches on surface passivation and chemical protection by thermal ALD-derived thin films have been performed[13], the majority of which focus on several common metal oxides like alumina and titania formed by TALD and their stability in various environments, especially in aqueous solutions for photoelectrochemical water splitting[14] and protection of stainless steel[15,16] or other metal substrates[17,18]. For example, Abdulagatov *et al*. deposited $Al_2O_3$ and $TiO_2$ on Cu and found that only $Al_2O_3$ or $TiO_2$ TALD films were insufficient to prevent copper from corrosion whereas the introduction of $TiO_2$ capping layer on $Al_2O_3$ films was more resilient to dissolution in water[18]. Strandwitz *et al*. have demonstrated TALD-derived MnO thin films can be used to stabilize n-Si photoelectrodes in chemically reactive conditions[19]. The chemical stability of TALD $Al_2O_3$ and $TiO_2$ films in different acidic, basic and neutral media, and the influence of post-deposition thermal treatment on different samples have been discussed[20]. These valuable results are helpful to expansive applications of organic electronic devices[21], stabilization of semiconductor photoanodes for water oxidation[22] and many other fields. However, to date, the work on PEALD metal oxide thin films as protective layers and anti-corrosion barriers is rather lacking[11,12,21].

In this paper, the chemical stability of as-deposited and post-annealed $TiO_2$, $ZrO_2$ and $HfO_2$ thin films derived from TALD and PEALD in various chemical liquid media, including 1 mol/L $H_2SO_4$, 1 mol/L HCl, 1 mol/L KOH, 1 mol/L KCl, and pure water, has been investigated and compared systematically. A series of analytical methods were used to characterize the change of thickness, chemical composition, structure and morphology of different samples. It is found that TALD/PEALD $HfO_2$ films exhibit the best chemical stability and anti-corrosion property without any change in thickness after long time immersion into various chemical solutions. The corrosion endurance of $HfO_2$ coating for 304 stainless steel (SS) in 1 mol/L KCl solution has been studied by *in-situ* electrochemical characterization.

## Results and Discussion

**Composition, morphology and structure.** Chemical composition of all as-deposited TALD and PEALD samples on Si was examined by XPS, as seen in Fig. 1. The strong doublet peaks of Ti *2p* (a), Zr *3d* (b) and Hf *4f* (c) with respective splitting energy of 5.7 eV, 2.4 eV, and 1.7 eV, and the strong O *1s* signal at 529.83 eV (d, only showing TALD and PEALD $HfO_2$) verify the formation of $TiO_2$, $ZrO_2$ and $HfO_2$ films by TALD and PEALD. Herein the weak O *1s* peak at 531.73 eV might come from the surface adsorption oxygen of $HfO_2$ films.

After 600 °C anneal, there is no obvious change in XPS spectra of $ZrO_2$ and $HfO_2$ films on Si. However, it is found that after 450 °C and 900 °C thermal treatment, the Si 2p signal appears on the surface of $TiO_2$ films/Si. Figure 2(a) records Si 2p narrow-scan XPS spectra of as-deposited, 450 °C and 900 °C annealed TALD- and PEALD-$TiO_2$ films surface. No Si 2p signal is detected on the surface of as-deposited TALD and PEALD samples. After 450 °C anneal, both samples exhibit Si 2p peaks at 101.98 eV, assigned to the chemical bond of Ti-O-Si. When further raising the anneal temperature to 900 °C, the Si 2p peaks shift to higher binding energy of 102.48 eV, indicating that more Si from substrate diffuses onto $TiO_2$ film surface and produce more Ti-silicate[23,24].

The XPS composition data attest that the atomic ratio of Si: Ti in the film surface is 0.25:1.00 at 450 °C and 0.31:1.00 at 900 °C for TALD samples, and in PEALD samples surface, the atomic ratio of Si: Ti is 0.28: 1.00 at 450 °C and 0.55:1.00 at 900 °C, respectively. The content of Si element on the surface of annealed $TiO_2$ films is rather high, so XPS depth analysis on as-deposited, 450 °C and 900 °C annealed TALD $TiO_2$ films was carried out by 1000 eV $Ar^+$ ions sputtering so as to clarify the source of Si, as indicated in Fig. 2(b–d). Atomic percent content of different elements was recorded every 60 s and the etch rate is around 0.56 Å/s. There is hardly Si signal for as-deposited $TiO_2$ film surface, but ~5 at% Si can be clearly observed on the annealed $TiO_2$ film surface. After the first etching process, Si content decreases to zero sharply with increased Ti and O contents, whose ratio is among 1.8~2.1, in basic agreement with the stoichiometric $TiO_2$. When it comes to 420 s, Si starts to emerge and increase gradually, and Ti and O contents become low. The interfacial diffusion layer of $(TiO_2)_m(SiO_2)_n$ is formed between $TiO_2$ films and Si substrate because $TiO_2$ film is thermodynamically unstable on Si substrate, which easily diffuses into the film and reacts with $TiO_2$ during thermal treatment, resulting in formation of Ti-silicate[25,26]. In addition, with the increase of anneal temperature, the thickness of interfacial diffusion layer becomes larger, which can be verified by the following thickness measurement.

FTIR spectra were also utilized to obtain the chemical group information of TALD-samples before and after thermal anneal, as recorded in Fig. 3. As-deposited sample show Ti-O bond at 614 $cm^{-1}$ with Ti-Cl bond at 811 $cm^{-1}$, C-Cl bond at 739 $cm^{-1}$ and C-OH bond at 1108 $cm^{-1}$, indicating the chlorine residue in film from $TiCl_4$ precursor and surface organic carbon contamination due to the lower deposition temperature of 200 °C. Besides Ti-O bond, 450 °C- and 900 °C-annealed $TiO_2$ films still display Ti-O-Si and Si-O modes of 1024 $cm^{-1}$ and 1148 $cm^{-1}$ with the disappearance of the Ti-Cl, C-Cl and C-OH bonds, confirming the Si element diffusion into films and removal of Cl residue and organic component after high temperature anneal.

SEM and AFM were conducted to characterize the film surface morphologies. Besides, the film thickness can be determined using spectroscopic ellipsometry and cross-section SEM images. The thicknesses of as-deposited and annealed TALD and PEALD $TiO_2$, $ZrO_2$ and $HfO_2$ films from spectroscopic ellipsometry before chemical test are summarized in Table 1. Evidently $ZrO_2$ and $HfO_2$ films become thinner after anneal, which can be ascribed

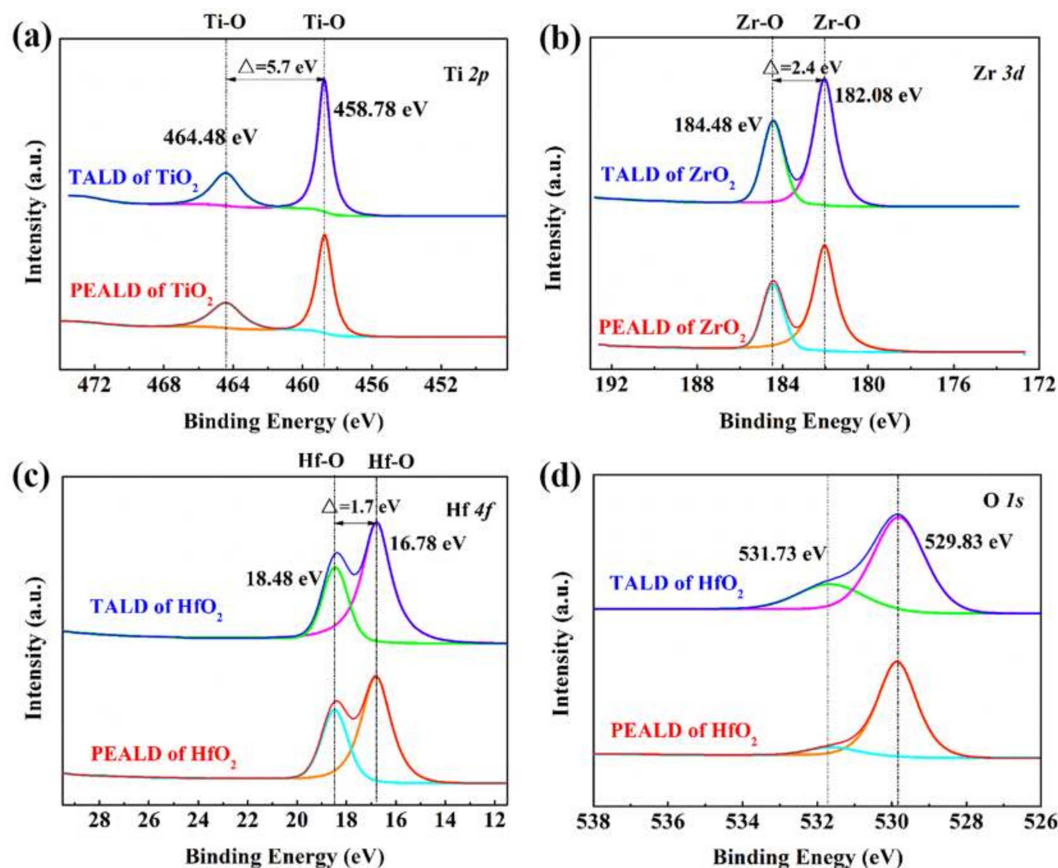


**Figure 1.** Narrow-scan Ti *2p*, Zr *3d* and Hf *4f* XPS spectra of as-deposited TALD and PEALD (**a**) $TiO_2$, (**b**) $ZrO_2$ and (**c**) $HfO_2$ films on Si. (**d**) Typical O *1s* XPS spectra of as-deposited TALD and PEALD $HfO_2$ films on Si.

to remove of oxygen vacancy and densification of films. However, $TiO_2$ films become thicker after thermal treatment, especially for 900 °C samples with remarkable thickness increase. This result is also verified by cross-section FESEM images of TALD $TiO_2$ films on Si substrate, as seen in Fig. 4.

Figure 5 is AFM images of as-deposited and annealed TALD and PEALD $TiO_2$ films. Thanks to the advantage of ALD technique, large area uniformity, the 200 °C as-deposited and 450 °C annealed films are of little roughness with root-mean-square (RMS) value of 0.2 nm, especially for samples formed by TALD. It can be seen from Fig. 5(c,f), after 3-hour 900 °C post annealing in $N_2$ atmosphere, surface morphology of TALD- and PEALD-$TiO_2$ films have greatly changed with small particles growing and gathering, the surface roughness increased to 1.8 nm and 3.1 nm respectively. Normally, thermal treatment at high temperature can enlarge grain size in the films, resulting in better crystallinity. Further discussion on structure of samples will be done according to XRD and XPS data.

Similarly, AFM images of as-deposited and annealed TALD $ZrO_2$ and $HfO_2$ films are presented in Fig. 6. After 600 °C annealing, the $ZrO_2$ films have relatively flat surfaces (RMS: 1.42 nm) without easily recognized grains, indicating poor crystallinity. The GIXRD pattern in Fig. 7(b) also proves this. Whereas 600 °C annealed $HfO_2$ films contain quite a few 20~30 nm particles with enhanced RMS of 2.56 nm. The XRD result in Fig. 7(c) reveals that stable $HfO_2$ monoclinic phase has been formed.

Due to thinner thickness of metal oxide films deposited by ALD technique, GIXRD with the help of synchrotron radiation was introduced to perform phase analysis. Figure 7 illustrates the GIXRD patterns of as-deposited and annealed TALD $TiO_2$, $ZrO_2$ and $HfO_2$ ultrathin films. As-deposited $TiO_2$ samples at 200 °C in Fig. 7(a) are amorphous without any diffraction peaks. 450 °C annealed samples show relatively stronger (101) peak at 25.2° and weak peaks of (004), (200), (105) and (211), which can be assigned to the anatase phase. In addition, a wide peak at 27.5° corresponds to the slight rutile phase. So the mixture of main anatase and slight rutile phases exists in 450 °C $TiO_2$ films. Nevertheless, after 900 °C anneal, the $TiO_2$ film crystallinity becomes worse, as confirmed by the reduced (101) peak intensity and some disappeared weak peaks. It has been reported that $TiO_2$ forms the anatase phase when thermal-treated between 300 and 500 °C, and then turns to the rutile structure above 800 °C anneal[27]. Herein the evident phase discrepancy can be attributed to the severe Si diffusion between $TiO_2$ ultrathin films and Si substrate, leading to the interfacial diffusion layer and the poor crystalline of $TiO_2$. Meanwhile, Si-doped $TiO_2$ films also prevent the transform from anatase to rutile phase. The XRD results are in good agreement with the mentioned-above XPS and FTIR analyses.

Comparing GIXRD patterns of $ZrO_2$ and $HfO_2$ films after 10-minute 600 °C RTA (Fig. 7(b,c)), obviously $HfO_2$ films have changed from amorphous to monoclinic phase with sharp peaks. The calculated grain size is 23.3 nm

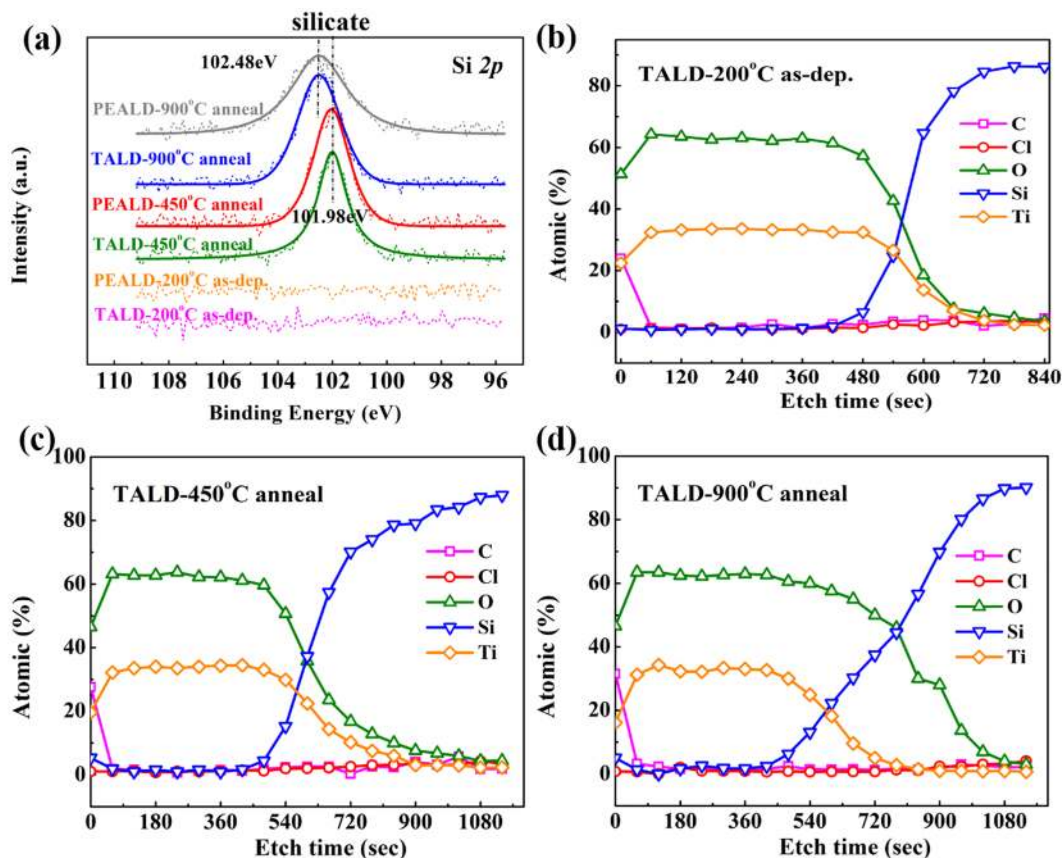


**Figure 2.** (**a**) Si 2p narrow-scan XPS spectra of as-deposited at 200 °C, 450 °C and 900 °C annealed TALD and PEALD $TiO_2$ films surface on Si. XPS depth profiles for (**b**) as-deposited at 200 °C, (**c**) 450 °C and (**d**) 900 °C annealed TALD-$TiO_2$ films on Si using $Ar^+$ ions etching.

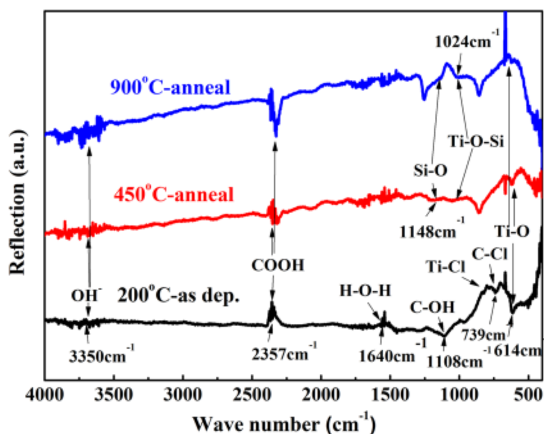


**Figure 3.** FTIR spectra of as-deposited at 200°, 450 °C and 900 °C annealed TALD $TiO_2$ films.

by Schereer equation, in consistent with AFM observation. While under the same anneal condition, the crystallinity of $ZrO_2$ films is not as good as that of $HfO_2$ and a weak and broad diffusion peak at 30.5° implies the trend of crystallinity.

**Chemical stability in chemical liquid media.** To study anti-corrosion property of group IV metal oxides, we immersed a subset of as-deposited and annealed TALD and PEALD samples in various chemical liquid media with a range of pH value, including acid solutions (1 mol/L $H_2SO_4$, 1 mol/L HCl), an alkaline solution (1 mol/L KOH) and neutral solutions (1 mol/L KCl, 18MΩ pure water). Film thickness was examined using spectroscopic ellipsometry after regular intervals. Figure 8 illustrates the thickness change dependence on immersion time for

| $TiO_2$ (1000 cycles) | TALD | | | PEALD | | |
|---|---|---|---|---|---|---|
| | as dep. | post-anneal | | as dep. | post-anneal | |
| | 200 °C | 450 °C | 900 °C | 200 °C | 450 °C | 900 °C |
| | 44.0 nm | 49.6 nm | 57.9 nm | 17.5 nm | 18.1 nm | 33.8 nm |
| $ZrO_2$ (500 cycles) | TALD | | | PEALD | | |
| | 250 °C-as dep. | | 600 °C-anneal | 250 °C-as dep. | | 600 °C-anneal |
| | 38.1 nm | | 34.8 nm | 40.1 nm | | 37.5 nm |
| $HfO_2$ (300 cycles) | TALD | | | PEALD | | |
| | 250 °C-as dep. | | 600 °C-anneal | 250 °C-as dep. | | 600 °C-anneal |
| | 37.9 nm | | 35.4 nm | 35.8 nm | | 32.2 nm |

**Table 1.** Thicknesses of as-deposited and annealed $TiO_2$, $ZrO_2$ and $HfO_2$ films prepared by TALD and PEALD from spectroscopic ellipsometry.

all as-deposited and post-annealed TALD/PEALD-$TiO_2$ films in various chemical environments, so as to evaluate the influence of anneal and deposition method on etching resistance of $TiO_2$ films.

From the point of view of film thickness variation, $TiO_2$ thin films in alkaline and neutral solutions of 1 mol/L KOH and 1 mol/L KCl are very stable, and the film thickness has hardly changed, even if as-deposited ones at 200 °C without post-anneal, as indicated in Fig. 8(c,d). In Fig. 8(e), as-deposited and 450 °C annealed $TiO_2$ samples in 18 MΩ water show a little slight thickness increase due to the hydration role; after 900 °C post-anneal, the film thickness basically keeps constant.

However, as-deposited $TiO_2$ thin films are unstable in acidic solutions with slow dissolution during the immersion duration, resulting in the visual change of the films in reflection color. The etch rates in 1 mol/L $H_2SO_4$ and 1 mol/L HCl in Fig. 8(a,b) are summarized in Table 2.

Evidently $H_2SO_4$ aqueous solution is more corrosive to as-deposited $TiO_2$ films than HCl solution at the same molar concentration, because sulfuric acid is a binary strong acid, which can ionize twice amount of $H^+$ of single hydrochloric acid. Moreover, the etch rate of as-deposited PEALD samples in acid drops by about 41% than that of as-deposited TALD ones, which can be ascribed to the fact that PEALD-derived samples have enhanced film density and lower impurity concentration due to the $O_2$ plasma's higher surface reactivity than only thermal energy-assisted process alone[28].

After annealed 450 °C and 900 °C for 3 h, the chemical stability of TALD and PEALD $TiO_2$ ultrathin films on Si is improved significantly with nearly unchanged thickness in strong acidic solutions over test period of 20 days in Fig. 8(a,b). As described above in Figs 2 and 7(a), the XPS and XRD results confirm that the longer time annealing at 450 °C and 900 °C for 3 h causes the Si diffusion into $TiO_2$ films to form the amorphous Ti-silicate containing partial crystalline anatase $TiO_2$ main phase. The amorphous Ti-silicate and crystalline $TiO_2$ exhibit better anti-acid corrosion performance than amorphous $TiO_2$. Especially, the formation of 5% Si-doped $TiO_2$ ultrathin layers on sample surfaces in Fig. 2(c,d) also plays an important role in enhancing the acid-endurance.

The thickness variation dependence on immersion time for all as-deposited and post-annealed TALD/PEALD-$ZrO_2$ films in various chemical environments are recorded in Fig. 9. Except for as-deposited TALD $ZrO_2$ films dissolving in 1 mol/L HCl with the etch rate of 1.06 nm/day, all other $ZrO_2$ samples exhibit better stability in different aqueous environments during the whole 20-day test, including annealed TALD and all PEALD samples. Herein, the influence of PEALD is much more significant without any etching than $TiO_2$ case for $O_2$ plasma contains more reactive radical and ionic species, beneficial to the corrosion-endurance $ZrO_2$ films' growth. Meanwhile annealing at high temperature may remove the residual impurities in films, leading to densification and crystallization trend of $ZrO_2$ films. This produces positive effects on improving anti-corrosion property of $ZrO_2$ films, as indicated in Fig. 9(b).

Figure 10 displays the anti-etching characteristics of all TALD and PEALD $HfO_2$ films in various chemical liquid media. Among three kinds of group IV metal oxides, $HfO_2$ films may be the best candidate as barrier layer in caustic environments, because after the long-time immersion in any acidic, alkaline and neutral solutions, all the $HfO_2$ samples show negligible change in thickness, no matter from TALD and PEALD or before and after anneal. So, we chose $HfO_2$ films as one candidate to further examine the corrosion resistance by electrochemical measurements.

**Electrochemical result.** We deposited 300 cycles $HfO_2$ films (~36 nm-thick) onto 304 stainless steels (304 SS) by TALD and PEALD. It was reported that the anti-corrosion properties of ALD $Al_2O_3$ thin films on steel could be improved by the $H_2$–Ar plasma pre-treatment[29]. In our experiment, 304 SS was treated by *in-situ* 50 s $H_2$-Ar plasma pulse before $HfO_2$ deposition so as to study the effect of the $H_2$ pre-treatment.

The polarization curves and Bode plots for the EIS data measured at OCP for the bare and coated 304 SS in 1 mol/L KCl are shown in Fig. 11. Only a peak at the corrosion potential can be observed in the polarization curves of each sample, indicating the $HfO_2$ coating films are electrochemically inert[30]. Compared with the bare 304 SS, the corrosion potential ($E_{corr}$) of TALD- and PEALD-$HfO_2$ coated 304 SS with and without $H_2$ plasma pretreatments, shifts to more negative potential, leading to improved corrosion resistance. Corrosion current density ($I_{corr}$) is another key factor to evaluate the corrosion reaction kinetics, which is usually proportional to the

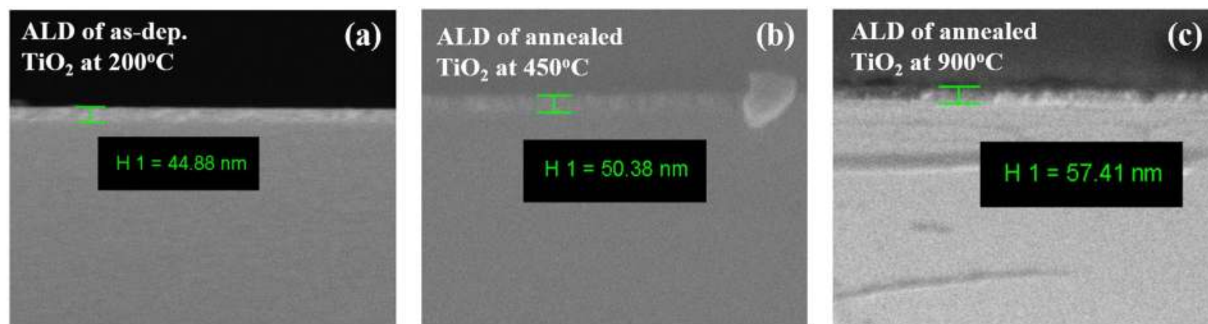


**Figure 4.** Cross-section FESEM images of TALD $TiO_2$ films before chemical test. (**a**) as-deposited at 200 °C. (**b**) 450 °C anneal. (**c**) 900 °C anneal.

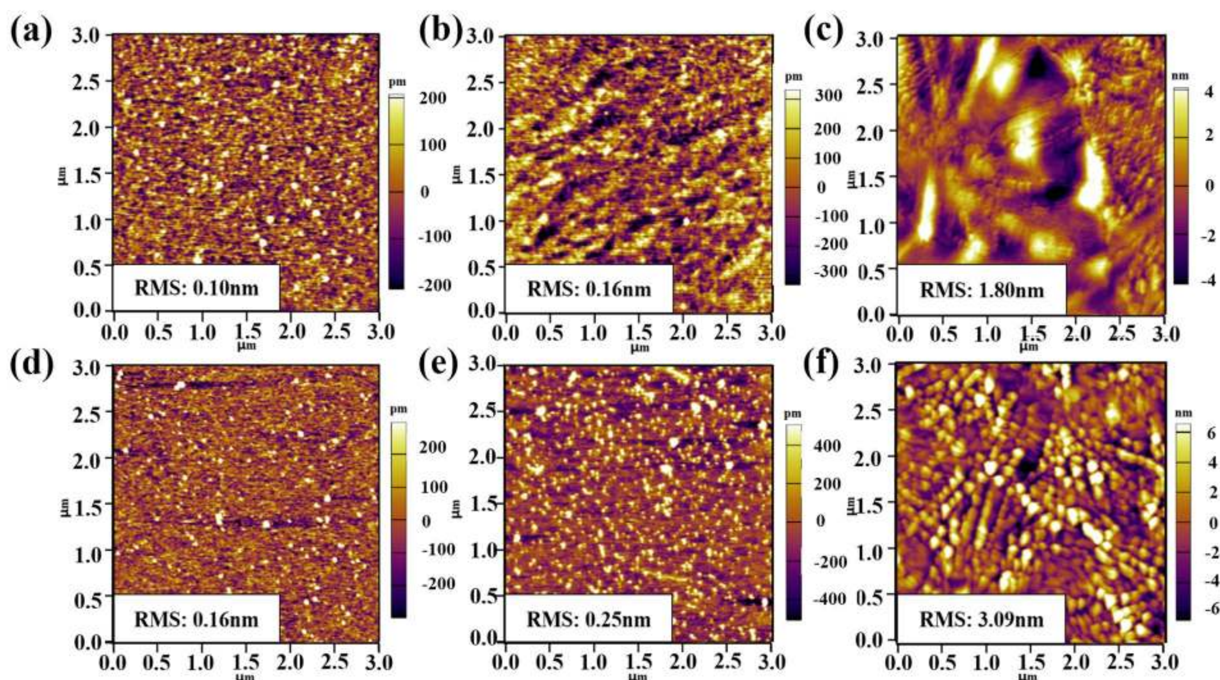


**Figure 5.** AFM images of as-deposited and annealed TALD and PEALD $TiO_2$ films. TALD: (**a**) as-deposited at 200 °C, (**b**) 450 °C anneal and (**c**) 900 °C anneal; PEALD: (**d**) as-deposited at 200 °C, (**e**) 450 °C anneal and (**f**) 900 °C anneal.

corrosion rate and can be obtained by Tafel fit analysis[16,31]. Additionally, polarization resistance ($R_p$) and porosity (P) are calculated and presented in Table 3, using Eqs 1 and 2.

The $HfO_2$ coatings lead to a marked decrease in corrosion current density ($I_{corr}$) from $1.09 \times 10^{-7}$ A/cm$^2$ for bare 304 SS to ~$10^{-10}$ A/cm$^2$ with three orders of drop. Accordingly, polarization resistance ($R_p$) increases by three orders of magnitude. The porosity (P) represents the nominal uncoated surface fraction of the 304 SS substrate based on the ratio of polarization resistance without and with $HfO_2$ coatings. The smaller the porosity (P) is, the better the corrosion resistance is. Among all samples, PEALD-$HfO_2$ coated 304 SS with $H_2$ plasma pretreatments exhibits the most encouraging anti-corrosion property with most negative potential of −0.48 V, lowest corrosion current density of $5.25 \times 10^{-11}$ A/cm$^2$, largest polarization resistance of $3.43 \times 10^8\ \Omega \cdot cm^2$ and smallest porosity of 0.01. This can be ascribed to the combination role of the $H_2$ plasma pre-treatment and the high $O_2$ plasma activity during PEALD. The removal of organic contamination and improvement of adhesion to the 304 SS caused by the $H_2$ plasma pre-treatment are beneficial to anti-corrosion property[29].

Electrochemical impedance spectra (Bode plots) of different samples are presented in Fig. 11(b). The $HfO_2$ coating properties are evaluated from low frequency to high frequency. Compared to the bare 304 SS, all $HfO_2$ coated 304 SS samples show a clear increase in the global impedance. Moreover, PEALD $HfO_2$ coated 304 SS samples maintain a higher phase angle in a wide frequency range from $10^{-2}$ Hz to $10^5$ Hz, giving better corrosion protection. Above all, the electrochemical results obtained from the LSV and the EIS confirm that PEALD $HfO_2$ coating onto $H_2$ plasma pretreated 304 SS has optimal corrosion-endurance.

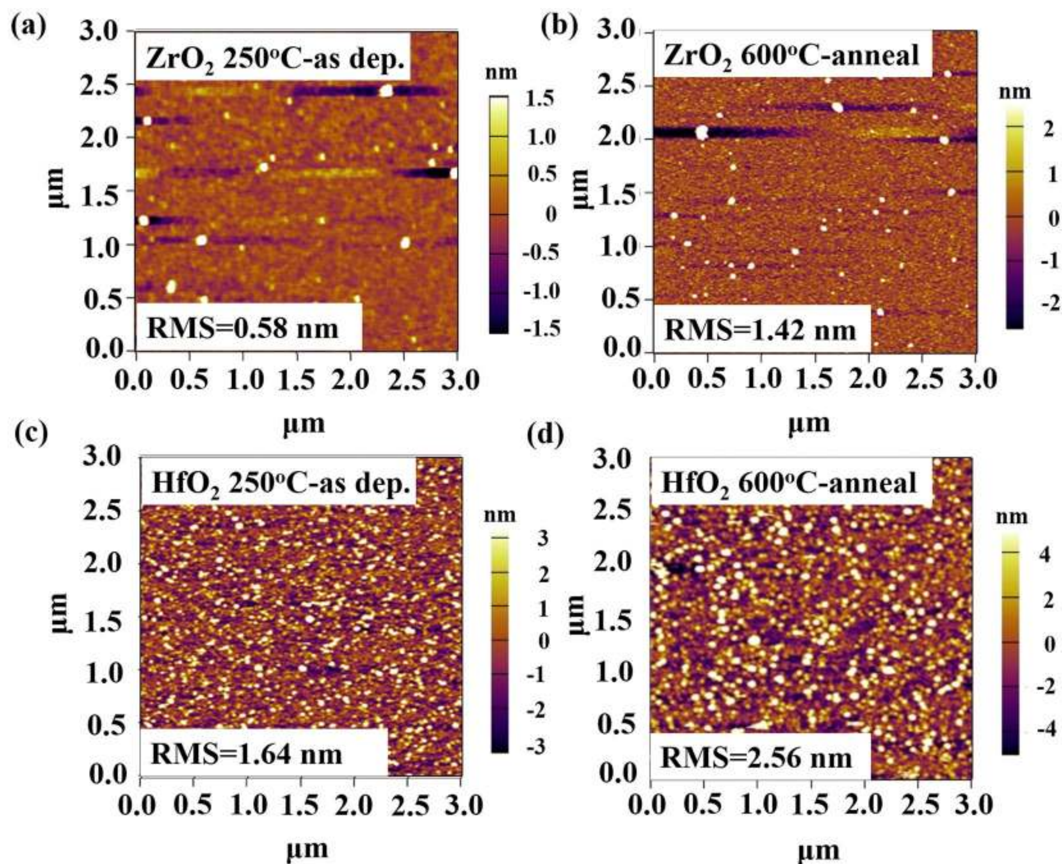


**Figure 6.** AFM images of as-deposited and annealed TALD $ZrO_2$ and $HfO_2$ films. (**a**,**c**) As-deposited at 250 °C; (**b**,**d**) 600 °C anneal.

## Conclusion

$TiO_2$, $ZrO_2$ and $HfO_2$ thin films were deposited on p-type Si (100) with nature oxide layer by the technique of TALD and PEALD. A variety of chemical liquid media including 1 mol/L $H_2SO_4$, 1 mol/L HCl, 1 mol/L KOH, 1 mol/L KCl, and 18 MΩ deionized water were used to test and compare chemical stability of all these as-deposited group IV metal oxides thin films, as well as post-annealed samples. In acidic solutions, TALD/PEALD $HfO_2$ films, whether annealed or not, exhibit the best chemical stability without any change in thickness after long time immersion. Except as-deposited TALD-$ZrO_2$ films with slowly etch rate of 1.06 nm/day in 1 mol/L HCl, all other $ZrO_2$ films show better anti-acid stability, indicating the role of introduction of plasma $O_2$ in PEALD and post-thermal treatment. As-deposited $TiO_2$ films are relatively unstable in acidic solutions of $H_2SO_4$ and HCl, where the etch rate is 1.39 nm/day and 0.82 nm/day for TALD ones, and 0.81 nm/day and 0.48 nm/day for PEALD ones, respectively. The etch rate of PEALD samples in acid solutions drops by about 41%, compared to TALD ones. After post-annealing, $TiO_2$ films have good corrosion endurance, which is ascribed to the crystallization transition from amorphous to anatase main phase and the formation of 5% Si-doped $TiO_2$ ultrathin layers on sample surfaces. In basic and neutral solutions, $HfO_2$, $ZrO_2$, and $TiO_2$ all show excellent corrosion resistance property with negligible change in thickness. Simultaneously, compared with bare 304 SS, 304 SS with $HfO_2$ coating shows enhanced anti-corrosion property, and 36 nm PEALD-$HfO_2$ is found to have a lower corrosion rate than TALD-$HfO_2$ ones, which is ascribed to the improved film quality when activated $O_2$ plasma is used. The pre-treatment of plasma $H_2$ to substrate of SS can reduce interfacial impurities and porosity of overlayers with increased corrosion resistance characteristics. Electrochemical analysis yields an exponential decay of the corrosion current density by four orders of magnitude. Above all, using PEALD technique, post-annealing process and plasma $H_2$ pre-treatment can improve the chemical stability and corrosion resistance of group IV metal oxide coatings. As a result, $HfO_2$, $ZrO_2$, and $TiO_2$ ultrathin films derived from TALD and PEALD allows various protective applications in several commonly-used chemical liquid environments.

## Materials and Methods

### Preparation of $TiO_2$, $ZrO_2$ and $HfO_2$ films by TALD and PEALD.

$TiO_2$ films were deposited at 200 °C, $ZrO_2$ and $HfO_2$ films were deposited at 250 °C, in a commercial Picosun SUNALE™ R-200 advanced PEALD system, which can be operated under PEALD and TALD modes. P-type Si (100) substrates (1 ~ 10 Ω · cm) were ultrasonically cleaned by acetone, alcohol and deionized water in turn without removing native oxide. $TiCl_4$, $Zr[N(C_2H_5)CH_3]_4$ (TEMAZ) and $Hf[N(C_2H_5)CH_3]_4$ (TEMAH) as metal precursors were used at room temperature, 150 °C and 155 °C, respectively. $H_2O$ and $O_2$ plasma were adopted as oxygen source for deposition of metal

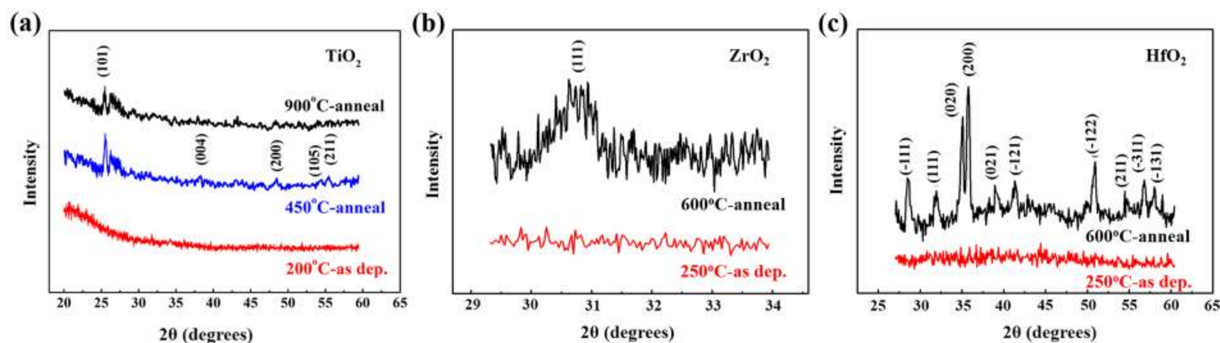


**Figure 7.** GIXRD patterns of as-deposited and annealed TALD $TiO_2$, $ZrO_2$ and $HfO_2$ ultrathin films.

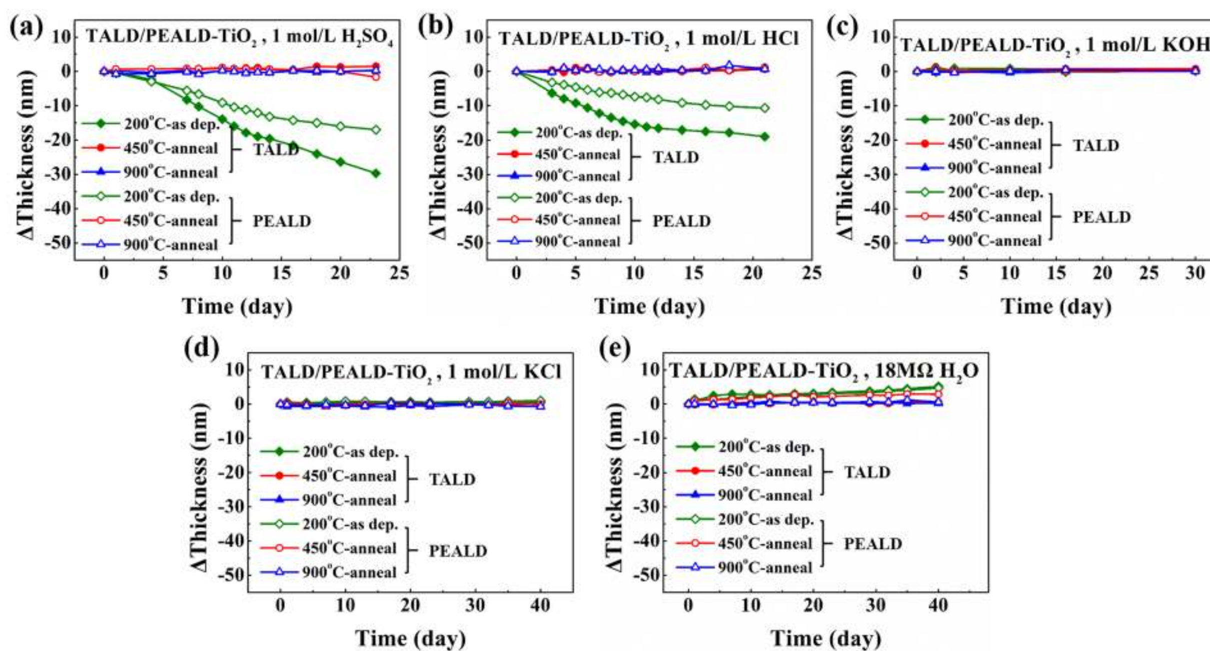


**Figure 8.** The thickness variation vs. immersion time for all as-deposited and post-annealed TALD/PEALD $TiO_2$ films in various chemical liquid media: (**a**) 1 mol/L $H_2SO_4$, (**b**) 1 mol/L HCl, (**c**) 1 mol/L KOH, (**d**) 1 mol/L KCl and (**e**) 18 MΩ water.

| | TALD-$TiO_2$ | | | PEALD-$TiO_2$ | | |
|---|---|---|---|---|---|---|
| | as dep. | post-anneal | | as dep. | post-anneal | |
| Solution | 200 °C | 450 °C | 900 °C | 200 °C | 450 °C | 900 °C |
| $H_2SO_4$ | 1.39 nm/day | — | — | 0.81 nm/day | — | — |
| HCl | 0.82 nm/day | — | — | 0.48 nm/day | — | — |

**Table 2.** Etch rates of TALD- and PEALD-$TiO_2$ films in 1 mol/L $H_2SO_4$ and 1 mol/L HCl.

oxide by TALD and PEALD, respectively, where remote plasma power and $O_2$ gas flow rate were 2,500 W and 160 sccm. For TALD-derived metal oxide thin films, all precursors' pulse time was 0.1 s, followed by a 4 s $N_2$ purge step to remove extra precursors and by-products. For PEALD-derived samples, the pulse and purge time of metal precursor kept unchanged, but pulse and purge time of plasma $O_2$ was extended to 13.5 s and 10 s, respectively.

All as-deposited samples were also annealed at high temperature to evaluate the effect of thermal treatment on chemical stability. Both TALD- and PEALD-$TiO_2$ films were heated in tube furnace at 450 °C and 900 °C for 3 h under $N_2$ atmosphere, while annealed $ZrO_2$ and $HfO_2$ films were made in $O_2$ environment at 600 °C for 10 min by rapid thermal annealing (RTA) to promote crystallization.

As-deposited and post-annealed samples were immersed in various chemical liquid media for various time, including 1 mol/L $H_2SO_4$, 1 mol/L HCl, 1 mol/L KOH, 1 mol/L KCl, and 18 MΩ deionized water. All the samples were stored in acid/alkaline-resistant boxes at room temperature in dark while control samples were placed in air.

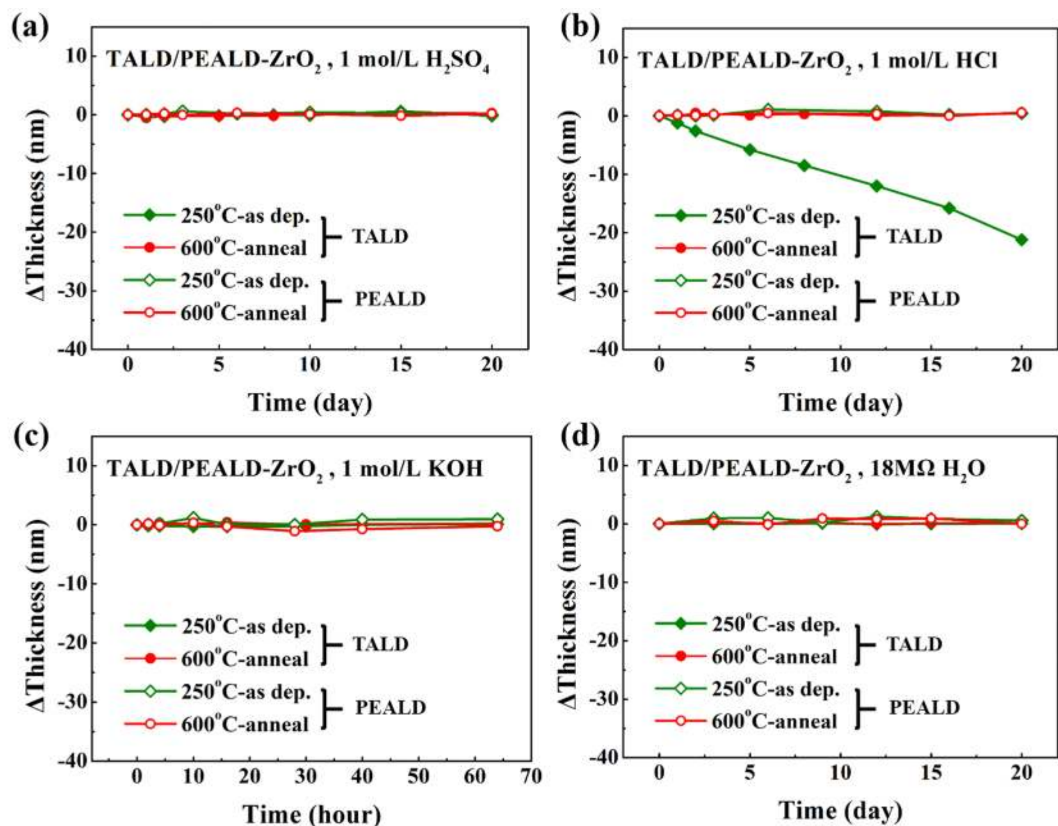


**Figure 9.** The thickness variation vs. time for all 250 °C as-deposited, 600 °C-annealed TALD/PEALD-$ZrO_2$ films in various chemical liquid media: (**a**) 1 mol/L $H_2SO_4$, (**b**) 1 mol/L HCl, (**c**) 1 mol/L KOH and (**d**) 18 MΩ water.

| | $H_2$ plasma pre-treatment | $E_{corr}$ (V) | $I_{corr}$ ($A \cdot cm^{-2}$) | $R_p$ ($\Omega \cdot cm^2$) | P (%) |
|---|---|---|---|---|---|
| Bare 304 SS | No | −0.17 | 1.09E-07 | 3.49E+05 | 100 |
| TALD-$HfO_2$ | No | −0.18 | 3.92E-10 | 2.77E+07 | 0.95 |
| | Yes | −0.24 | 3.55E-10 | 4.73E+07 | 0.24 |
| PEALD-$HfO_2$ | No | −0.26 | 1.78E-10 | 9.29E+07 | 0.15 |
| | Yes | −0.48 | 5.25E-11 | 3.43E+08 | 0.01 |

**Table 3.** Parameters related to the polarization curves in Fig. 11(a) for untreated bare 304 SS and TALD- and PEALD-$HfO_2$ coated 304 SS with and without $H_2$ plasma pretreatments.

**Characterization.** The physical thickness of films (before and after immersion) was estimated by spectroscopic ellipsometry (Sopra GES-5) at an incidence angle of 75° and with wavelengths between 300 nm to 800 nm at increments of 10 nm. The data were then fit using the Cauchy (epsi) model for $TiO_2$, $ZrO_2$ and $HfO_2$ films to acquire thickness value. A fixed native $SiO_2$ layer (1~2 nm) was considered in the model at the Si-metal oxide interface using the software of WinElli. X-ray photoelectron spectroscopy (XPS, Thermo Fisher K-Alpha, USA) was explored to characterize the chemical state and component of samples, using a monochromatic Al *Kα* source ($h\nu = 1,486.6$ eV) for excitation of photoelectrons and binding energy scale was calibrated using C 1 s peak at 284.6 eV. Fourier transform infrared spectroscopy (FTIR) was used to obtain the chemical group information of the thin films using a pristine Si substrate as a reference. Crystallinity and phase structures of the films were analyzed by grazing incidence X-ray diffraction (GIXRD, Shanghai Synchrotron Radiation Facility, BL14B1) system with the light source energy of 10k eV and grazing incidence of 0.12° due to the extremely thin thickness of the films. The surface topography was recorded by atomic force microscopy (AFM, Cypher, USA) and field emission scanning electron microscopy (FESEM, Zeiss Ultra 55, German). The cross-section FESEM image was also recorded to corroborate the thickness of samples.

Electrochemical measurements were performed by CHI660E electrochemical workstation and three-electrode tests where bare or coated 304 SS was used as the working electrode, a platinum wire as the counter electrode, saturated Ag/AgCl solution as a reference, and 1 mol/L KCl as the electrolyte and corrosion solution. 704 silicone

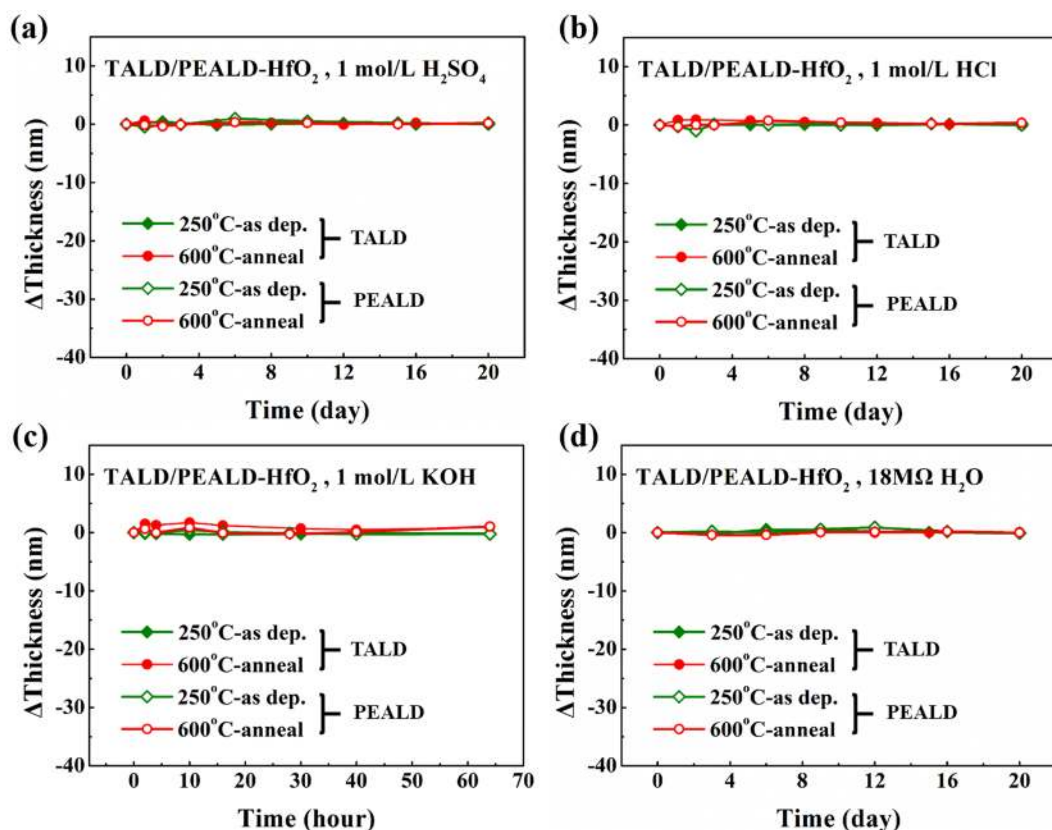


**Figure 10.** The thickness variation vs. time for all 250 °C as-deposited, 600 °C-annealed TALD/PEALD-$HfO_2$ films in various chemical liquid media: (**a**) 1 mol/L $H_2SO_4$, (**b**) 1 mol/L HCl, (**c**) 1 mol/L KOH and (**d**) 18 MΩ water.

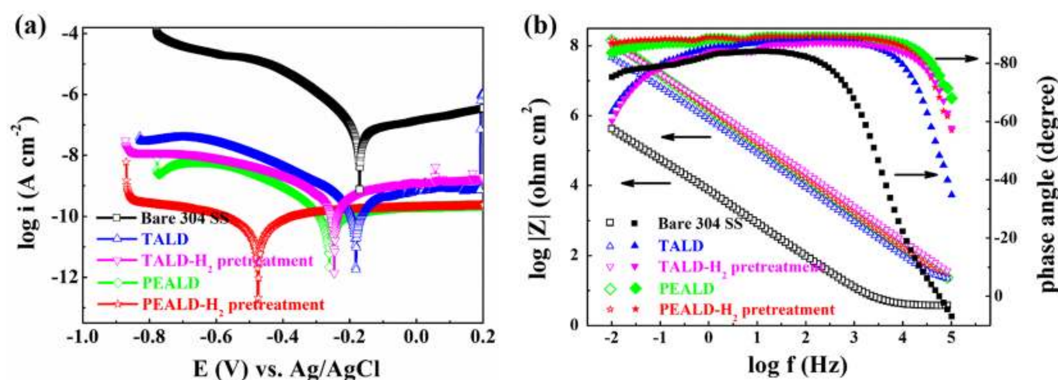


**Figure 11.** (**a**) Polarization curves and (**b**) Bode plots of untreated bare 304 SS and TALD- and PEALD-$HfO_2$ coated 304 SS with and without $H_2$ plasma pretreatments.

rubber was used to encapsulate the surface of the sample. The reverse side of the sample was sealed after the extraction of the Al electrode ears equipped with the electrochemical workstation. Only a square area of about $1 \times 1\,cm^2$ was left on the front for testing. Figure 12 shows the experimental setup for electrochemical measurements including electrochemical workstation, three-electrode test and sample package picture.

During measurement, the open circuit potential (OCP) was detected for one hour to attain a steady potential, then the electrochemical impedance spectroscopy (EIS) measurements were conducted in a frequency range of $10^{-2}$ to $10^5$ Hz at OCP. The linear sweep voltammetry (LSV) data were collected at a rate of 20 mV/min and the corrosion potentials, corrosion currents, polarization resistances and porosities were calculated based on the polarization curves using the Stern-Geary equation[30]

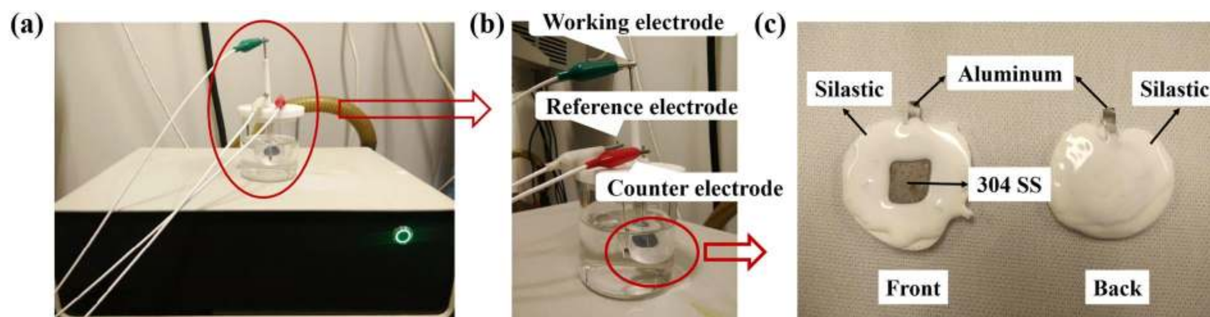


**Figure 12.** Experimental setup for electrochemical measurements including (**a**) electrochemical workstation, (**b**) three-electrode test and (**c**) sample package picture.

$$R_P = \frac{b_a b_c}{i_{corr} \ln(10)(b_a + b_c)} \quad (1)$$

where $b_a$ and $b_c$ are the slopes of the anodic and cathodic branches of the Tafel plot, respectively. The electrochemical porosity of the films deposited onto SS was obtained by comparing $R_p$ of coated and bare SS[29].

$$P = \frac{R_{p-bare}}{R_{p-ALD}} \times 100\% \quad (2)$$

## References


1. George, S. M. Atomic layer deposition: an overview. *Chem. Rev.* **110**, 111–131 (2010).
2. Lim, J. W., Yun, S. J. & Lee, J. H. Characteristics of $TiO_2$ films prepared by ALD with and without plasma. *Electrochem. Solid-State Lett.* **7**, F73–F76 (2004).
3. Aarik, J. *et al*. Phase transformations in hafnium dioxide thin films grown by atomic layer deposition at high temperatures. *Appl. Surf. Sci.* **173**, 15–21 (2001).
4. Niinistö, J., Kukli, K., Heikkilä, M., Ritala, M. & Leskelä, M. Atomic layer deposition of high-k oxides of the group 4 metals for memory applications. *Adv. Eng. Mater.* **11**, 223–234 (2009).
5. Zhang, W. *et al*. Bipolar Resistive Switching Characteristics of $HfO_2/TiO_2/HfO_2$ Trilayer-Structure RRAM Devices on Pt and TiN-Coated Substrates Fabricated by Atomic Layer Deposition. *Nanoscale Res. Lett.* **12**, 393–1~11 (2017).
6. Cao, Y. Q. *et al*. Improved thermal stability and electrical properties of atomic layer deposited $HfO_2$/AlN high-k gate dielectric stacks on GaAs. *J. Vac. Sci. Technol. A* **33**, 01A136–1~6 (2015).
7. Puurunen, R. L. Surface chemistry of atomic layer deposition: A case study for the trimethylaluminium/water process. *J. Appl. Phys.* **97**, 121301 (2015).
8. Miikkulainen, V., Leskela, M., Ritala, M. & Puurunen, R. L. Crystallinity of inorganic films grown by atomic layer deposition: Overview and general trends. *J. Appl. Phys.* **113**, 021301 (2013).
9. Profijt, H. B., Potts, S. E., De Sanden, M. C. & Kessels, W. M. Plasma-assisted atomic layer deposition: basics, opportunities, and challenges. *J. Vac. Sci. Technol. A* **29**, 050801 (2011).
10. Kim, H. Characteristics and applications of plasma enhanced-atomic layer deposition. *Thin Solid Films* **519**, 6639–6644 (2011).
11. Potts, S. E. *et al*. Ultra-thin aluminium oxide films deposited by plasma-enhanced atomic layer deposition for corrosion protection. *J. Electrochem. Soc.* **158**, C132–C138 (2011).
12. Potts, S. E. *et al*. Low temperature plasma-enhanced atomic layer deposition of metal oxide thin films. *J. Electrochem. Soc.* **157**, P66–P74 (2010).
13. Matero, R. *et al*. Atomic layer deposited thin films for corrosion protection. *J. Phys. IV* **9**, 493–499 (1999).
14. Hu, S. *et al*. Amorphous $TiO_2$ coatings stabilize Si, GaAs, and GaP photoanodes for efficient water oxidation. *Science* **344**, 1005–1009 (2014).
15. Marin, E., Lanzutti, A., Guzman, L. & Fedrizzi, L. Corrosion protection of AISI 316 stainless steel by ALD alumina/titania nanometric coatings. *J. Coat. Technol. Res.* **8**, 655–659 (2011).
16. Shan, C. X., Hou, X. H. & Choy, K. L. Corrosion resistance of $TiO_2$ films grown on stainless steel by atomic layer deposition. *Surf. Coat. Technol.* **202**, 2399–2402 (2008).
17. Mirhashemihaghighi, S. *et al*. Corrosion protection of aluminium by ultra-thin atomic layer deposited alumina coatings. *Corros. Sci.* **106**, 16–24 (2016).
18. Abdulagatov, A. I. *et al*. $Al_2O_3$ and $TiO_2$ Atomic Layer Deposition on Copper for Water Corrosion Resistance. *ACS Appl. Mat. Interfaces* **3**, 4593–4601 (2011).
19. Strandwitz, N. C. *et al*. Photoelectrochemical behavior of n-type Si (100) electrodes coated with thin films of manganese oxide grown by atomic layer deposition. *J. Phys. Chem. C* **117**, 4931–4936 (2013).
20. Correa, G. C., Bao, B. & Strandwitz, N. C. Chemical stability of titania and alumina thin films formed by atomic layer deposition. *ACS Appl. Mat. Interfaces* **7**, 14816–14821 (2015).
21. Kim, L. H. *et al*. $Al_2O_3/TiO_2$ nanolaminate thin film encapsulation for organic thin film transistors via plasma-enhanced atomic layer deposition. *ACS Appl. Mat. Interfaces* **6**, 6731–6738 (2014).
22. Chen, Y. W. *et al*. Atomic layer-deposited tunnel oxide stabilizes silicon photoanodes for water oxidation. *Nat. mater.* **10**, 539–544 (2011).
23. Klein, T. M. *et al*. Evidence of aluminum silicate formation during chemical vapor deposition of amorphous $Al_2O_3$ thin films on Si(100). *Appl. Phys. Lett.* **75**, 4001 (1999).
24. Zhang, W. Q., Huang, L. Y., Li, A. D. & Wu, D. $Hf_xZr_{1-x}O_2$ films chemical vapor deposited from a single source precursor of anhydrous $Hf_xZr_{1-x}(NO_3)_4$. *J. Cryst. Growth.* **346**, 0–16 (2012).

25. Wilk, G. D., Wallace, R. M. & Anthony, J. M. Hafnium and zirconium silicates for advanced gate dielectrics. *J. Appl. Phys.* **87**, 484–492 (2000).
26. Gilmer, D. C. *et al*. Low Temperature CVD of Crystalline Titanium Dioxide Films Using Tetranitratotitanium(IV). *Chem. Vap. Deposition* **4**, 9–11 (1998).
27. Lim, G. T. & Kim, D. Characteristics of $TiO_x$ films prepared by chemical vapor deposition using tetrakis-dimethyl-amido-titanium and water. *Thin Solid Films* **498**, 254–258 (2006).
28. Yun, S. J., Lim, J. W. & Lee, J. H. Effect of plasma on characteristics of zirconium oxide films deposited by plasma-enhanced atomic layer deposition. *Electrochem. Solid-State Lett.* **8**, F47–F50 (2005).
29. Harkonen, E. *et al*. Hydrogen–argon plasma pre-treatment for improving the anti-corrosion properties of thin $Al_2O_3$ films deposited using atomic layer deposition on steel,. *Thin Solid Films* **534**, 384–393 (2013).
30. Daubert, J. S. *et al*. Corrosion protection of copper using $Al_2O_3$, $TiO_2$, ZnO, $HfO_2$, and $ZrO_2$ atomic layer deposition. *ACS Appl. Mat. Interfaces* **9**, 4192–4201 (2017).
31. Díaz, B. *et al*. Low-temperature atomic layer deposition of $Al_2O_3$ thin coatings for corrosion protection of steel: Surface and electrochemical analysis. *Corros. Sci.* **53**, 2168–2175 (2011).

## Acknowledgements
This project is supported by the Natural Science Foundation of China (51571111, 51721001, 51802150) and Jiangsu Province (BK2016230, and BK20170645), a grant from the State Key Program for Basic Research of China (2015CB921203), the general grant from the China Postdoctoral Science Foundation (2017M611778), and the Central Universities (021314380075). Dr. Ai-Dong Li also thanks the support from the open project of NLSSM (M30038).

## Author Contributions
M.L. and Z.X.J. carried out the sample fabrication and characterization of SEM and XRD, W.Z. and Y.H.B. conducted the XPS, AFM and FTIR tests. M.L. and Y.Q.C. conducted the chemical stability test and electrochemical measurement. W.M.L., D.W. and A.D.L. participated in the discussion of results. M.L. drafted the manuscript. A.D.L. supervised the whole work and revised the manuscript. All authors critically read and commented on the manuscript.

## Additional Information
**Competing Interests:** The authors declare no competing interests.

**Publisher's note:** Springer Nature remains neutral with regard to jurisdictional claims in published maps and institutional affiliations.

**Open Access** This article is licensed under a Creative Commons Attribution 4.0 International License, which permits use, sharing, adaptation, distribution and reproduction in any medium or format, as long as you give appropriate credit to the original author(s) and the source, provide a link to the Creative Commons license, and indicate if changes were made. The images or other third party material in this article are included in the article's Creative Commons license, unless indicated otherwise in a credit line to the material. If material is not included in the article's Creative Commons license and your intended use is not permitted by statutory regulation or exceeds the permitted use, you will need to obtain permission directly from the copyright holder. To view a copy of this license, visit http://creativecommons.org/licenses/by/4.0/.

© The Author(s) 2019